

Research Paper

Cite this article: Mu T, Song Y (2020). Target range–angle estimation based on time reversal FDA-MIMO radar. *International Journal of Microwave and Wireless Technologies* **12**, 267–275. <https://doi.org/10.1017/S1759078719001351>

Received: 12 June 2019

Revised: 14 September 2019

Accepted: 17 September 2019

First published online: 21 October 2019


Key words:

Multiple-input and multiple-output; frequency diverse array; time reversal; range-angle estimation

Author for correspondence:

Yaoliang Song, E-mail: ylsong@njjust.edu.cn

Target range–angle estimation based on time reversal FDA-MIMO radar

Tong Mu  and Yaoliang Song

School of Electronic and Optical Engineering, Nanjing University of Science and Technology, Nanjing, China

Abstract

Different from traditional multiple-input and multiple-output (MIMO) radar, the frequency diverse array MIMO (FDA-MIMO) radar generates beampattern that is dependent on both range and angle, making it applicable for joint range–angle estimation of targets. In this paper, we propose a novel time reversal based FDA-MIMO (TR-FDA-MIMO) approach for target detection. Based on the time reversal theory, the TR-FDA-MIMO signal model is established, the TR transmitting–receiving and signal processing procedure are analyzed, and the resulting range–angle spectra for targets imaging are acquired by utilizing the multiple signal classification algorithm. Numerical simulations are carried out for both single and multiple targets cases. The imaging resolution and robustness to the noise of the proposed approach are investigated and results are compared with conventional FDA-MIMO radar. It turned out that by cooperating with TR, the performance of FDA-MIMO radar for target range–angle estimation is effectively enhanced, consequently improving its applicability in practical target-detecting cases.

Introduction

The flexibility of multiple-input and multiple-output (MIMO) radar in signal waveform and array structure brings increased degrees-of-freedom (DoFs) and spatial diversity gain, leading to enhancement of target detecting accuracy and resolution. MIMO radar has gained wide attention in recent years due to its promising advantages [1–3]. However, the beampattern of traditional MIMO radar only depends on the angle, which results in difficulty in distinguishing targets and suppressing interferences located in the same direction but different ranges.

The frequency diverse array (FDA) provides new ideas for radar system design by introducing a tiny frequency increment among array elements. The main difference between FDA and phased array (PA) is that the transmit beampattern of FDA changes as a function of range, angle, and time, which is favorable for locating targets and suppressing range-dependent interferences. Thus, FDA has been extensively investigated since it was proposed in 2006 [4–6]. The periodic modulation properties of FDA were studied in [7]. A logarithmically increasing frequency offset was introduced in [8] to decouple the beampattern, but it causes reduced range–angle resolution and increased sidelobes. In [9], time-modulated frequency offset was proposed to solve the time-variance problem in FDA, and some other studies concerning the same issue were presented in [10–13]. However, FDA cannot be directly used as a receiving array for target localization due to the range–angle coupling. Naturally, advantages of FDA in range-dependent beampattern and MIMO in increased DoFs are combined to realize unambiguous target range–angle estimation. Joint parameters estimation based on FDA-MIMO was proposed in [14], and suppressing range-dependent interferences using FDA-MIMO was presented in [15]. The Cramer–Rao lower bound, mean square error, and resolution performance of FDA-MIMO radar were derived in [16].

The time reversal (TR) technique exploits the invariance of wave equation in lossless and time-invariant media to implement the reversion, retransmission, and focusing of signals [17]. Recently, TR has been widely utilized in radar applications for its temporal-spatial focusing characteristic and statistical stability [18–20]. In [21], TR was combined with MIMO to improve radar performance in multipath rich cases. In [22], a TR-MIMO algorithm was proposed for direction of arrival (DOA) estimation, and the multi-target signal model for TR-MIMO radar was analyzed in [23]. The method proposed in [24] applies the compressive sensing and TR to MIMO radar for target detection in a rich clutter environment. However, existing studies mainly focus on the angle acquirement of target, while the problem of range parameter estimation and range-dependent interferences mitigation cannot be solved effectively, limiting the potential of TR-MIMO radar.

In this paper, we introduce time reversal to FDA-MIMO radar and propose a new TR-based FDA-MIMO (TR-FDA-MIMO) scheme for enhanced target detection. Orthogonal signals with a small frequency increment are used for transmission, which makes the transmit beampattern or steering vector dependent on both range and angle.

After target returns reception, instead of performing signal processing as in conventional FDA-MIMO radar, the received signals are time reversed and retransmitted by corresponding antennas. Then, matched filtering is conducted to the retrieved signals for computing the signal matrix for target parameters estimation. At last, the commonly adopted multiple signal classification (MUSIC) algorithm is employed for range-angle spectra imaging [25]. Numerical simulations are carried out to verify the effectiveness of the proposed approach. Comparative results between TR-FDA-MIMO and FDA-MIMO radars for both single and multiple targets are analyzed, demonstrating the superiority of the new method in target detection, especially in noise cases.

Mechanism of TR-FDA-MIMO radar

Transmit beampattern of basic FDA

Different from PA that transmits signals with identical frequency, there exists a small frequency increment in the carrier frequency across antennas in FDA. Consider a uniform linear array (ULA) consisting of M elements with spacing d . The signal radiated by the m th antenna can be represented as

$$x_m(t) = e^{j2\pi f_m t}, \quad m = 0, 1, \dots, M - 1, \quad (1)$$

where f_m is defined as

$$f_m = f_0 + m\Delta f, \quad (2)$$

where f_0 is the reference carrier frequency and Δf is the frequency increment. The overall signal observed at a far-field point with coordinate (r, θ) is

$$X(t; r, \theta) = \sum_{m=0}^{M-1} x_m\left(t - \frac{r_m}{c}\right), \quad (3)$$

where c is the speed of light in free space and r_m is the distance from the point to the m th antenna. Take far-field approximation $r_m \approx r - md\sin\theta$ into consideration and substitute (1) and (2) into (3), we have

$$\begin{aligned} X(t; r, \theta) &= \sum_{m=0}^{M-1} e^{j2\pi(f_0 + m\Delta f)[t - (r - md\sin\theta)/c]} \\ &\approx e^{j2\pi f_0(t - r/c)} \sum_{m=0}^{M-1} e^{j2\pi m\Delta f(t - r/c)} e^{j2\pi f_0 md\sin\theta/c}, \end{aligned} \quad (4)$$

where r and θ are the range and azimuth angle of the point relative to the first antenna, respectively. Note that the term $e^{j2\pi\Delta f m^2 d\sin\theta/c}$ has been neglected from (4) since $\Delta f \ll f_0$. Thus, the array factor can be written as

$$AF(t; r, \theta) = \sum_{m=0}^{M-1} e^{j2\pi m\Delta f(t - r/c)} e^{j2\pi f_0 md\sin\theta/c} \quad (5)$$

and accordingly the FDA transmit steering vector is given by

$$\mathbf{a}(r, \theta) = [1, e^{j\varphi}, \dots, e^{j(M-1)\varphi}]^T, \quad (6)$$

where $\varphi = 2\pi f_0 d\sin\theta/c - 2\pi\Delta f r/c$ and $(\cdot)^T$ denotes the transposition.

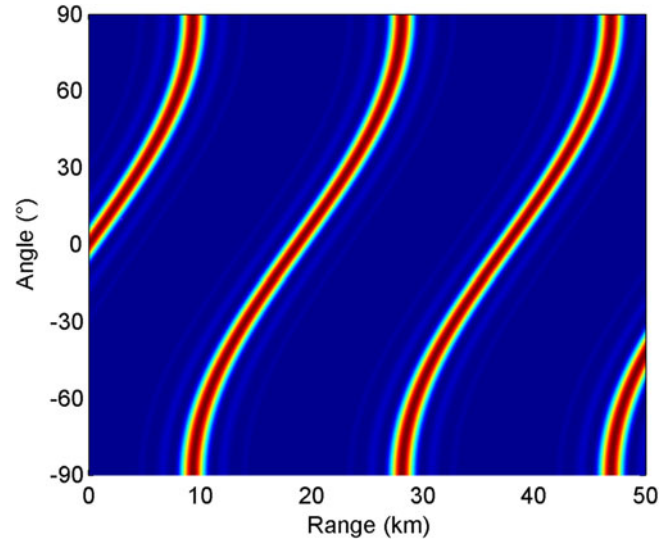


Fig. 1. Transmit beampattern of FDA radar.

Figure 1 shows a basic FDA transmit beampattern distributed in the range-angle domain. The input parameters for this beampattern are: the carrier frequency is $f_0 = 10$ GHz, the frequency increment is $\Delta f = 16$ KHz, and the number of antennas is $M = 10$. It is clearly seen that the FDA transmit beampattern is a function of range and angle and has S-shape because of coupling, which can be properly exploited for joint range-angle estimation of targets.

Signal model of FDA-MIMO radar

Now consider a co-located FDA-MIMO radar that contains M transmitting elements and N receiving elements. Compared with the basic FDA radar, the m th emitted signal is modified as

$$x_m(t) = \phi_m(t)e^{j2\pi f_m t}, \quad 0 \leq t \leq T, \quad (7)$$

where T is the signal duration, and $\phi_m(t)$ is the baseband modulation signal that satisfies the orthogonality condition, i.e.

$$\int_0^T \phi_m(t)\phi_{m'}^*(t - \tau)dt = 0, \quad m \neq m', \quad \forall \tau, \quad (8a)$$

$$\int_0^T \phi_m(t)\phi_m^*(t)dt = 1, \quad m = m', \quad (8b)$$

where $(\cdot)^*$ denotes the conjugation and τ is the time shift. Here, although the form of $\phi_m(t)$ is not defined in the theoretical derivation, specific modulation functions should be used in the numerical simulation. Actually, the radar performance can be affected by the waveform modulation so transmit waveform design and optimization for FDA-MIMO radar is also significant; however, this issue is beyond the scope of this paper.

The transmitted signals are reflected by the target located at (r, θ) and then recorded by the receiving array. The signal received by the n th antenna can be written as

$$y_n(t) = \sum_{m=0}^{M-1} \phi_m(t - \tau_{nr})e^{j2\pi f_m(t - \tau_{nr})}, \quad n = 0, 1, \dots, N - 1, \quad (9)$$

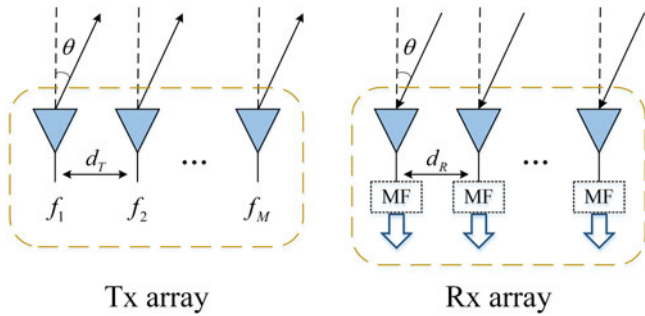


Fig. 2. Schematic diagram of FDA-MIMO radar.

where τ_{tr} is the total time delay corresponding to signal propagation from the m th transmitting element to the n th receiving element, expressed as

$$\tau_{tr} = \frac{2r - md_T \sin \theta - nd_R \sin \theta}{c}, \tag{10}$$

where d_T and d_R are the element spacings of transmitting and receiving array, respectively. Substituting (10) into (9) yields

$$\begin{aligned} y_n(t) &= \sum_{m=0}^{M-1} \phi_m [t - (2r - md_T \sin \theta - nd_R \sin \theta)/c] e^{j2\pi f_m [t - (2r - md_T \sin \theta - nd_R \sin \theta)/c]} \\ &\approx e^{j2\pi f_0 (t - 2r/c)} e^{j2\pi md_R \sin \theta / \lambda_0} \\ &\times \sum_{m=0}^{M-1} \phi_m [t - (2r - md_T \sin \theta - nd_R \sin \theta)/c] e^{j2\pi \Delta f m (t - 2r/c)} e^{j2\pi md_T \sin \theta / \lambda_0}, \end{aligned} \tag{11}$$

where $\lambda_0 = c/f_0$ is the carrier wavelength. Similar to (4), quadratic terms related to the element index have been neglected from (11).

After down converting and matched filtering, the output of the n th receiving element for the m th transmitting element is represented by

$$y_{m,n}(r, \theta) = \xi e^{j2\pi md_R \sin \theta / \lambda_0} e^{-j4\pi \Delta f m r / c} e^{j2\pi md_T \sin \theta / \lambda_0}, \tag{12}$$

where ξ is the complex scattering coefficient of the target.

In an FDA-MIMO radar, the range changing characteristic provided by FDA and the angle changing characteristic provided by MIMO are effectively combined, resulting in synchronous range and angle estimation. The schematic diagram of FDA-MIMO radar is illustrated in Fig. 2.

Range-angle estimation using TR-FDA-MIMO radar

Now we present the TR-FDA-MIMO signal model and perform target range-angle estimation based on the proposed scheme. For expression conciseness, vector form is adopted in signal derivation, and meanwhile noise is taken into account.

Assume there are P incoherent targets located at (r_p, θ_p) in the far field with $p = 0, 1, \dots, P-1$. The transmitting signal vector is

$$\mathbf{X}(t) = [x_0(t), x_1(t), \dots, x_{M-1}(t)]^T \tag{13}$$

and the corresponding receiving signal vector is expressed as

$$\mathbf{Y}(t) = \sum_{p=1}^P \mathbf{b}(\theta_p) \beta_p \mathbf{a}^T(r_p, \theta_p) \mathbf{X}(t) + \mathbf{n}_y(t), \tag{14}$$

where β_p is the complex scattering coefficient of the p th target. $\mathbf{n}_y(t)$ is the white Gaussian noise (WGN) vector with mean and variance being zero and σ^2 respectively. $\mathbf{b}(\theta)$ is the angle-dependent receiving steering vector which is given by

$$\mathbf{b}(\theta) = [1, e^{j\varphi_b}, \dots, e^{j(N-1)\varphi_b}]^T, \tag{15}$$

where $\varphi_b = 2\pi d_R \sin \theta / \lambda_0$. $\mathbf{a}(r, \theta)$ is the range-angle-dependent transmitting steering vector which is given by

$$\mathbf{a}(r, \theta) = [1, e^{j\varphi_a}, \dots, e^{j(M-1)\varphi_a}]^T, \tag{16}$$

where $\varphi_a = 2\pi d_T \sin \theta / \lambda_0 - 4\pi \Delta f r / c$.

For general FDA-MIMO radar, the output signal of the matched filter is

$$\mathbf{Y}_{MF} = E\{\mathbf{Y}(t)\mathbf{X}^H(t)\} = \sum_{p=1}^P \beta_p \mathbf{b}(\theta_p) \mathbf{a}^T(r_p, \theta_p) + \mathbf{N}_y, \tag{17}$$

where $E\{\cdot\}$ denotes the mathematical expectation, $(\cdot)^H$ denotes the conjugate transposition, and \mathbf{N}_y is the matched filter output of $\mathbf{n}_y(t)$. For the proposed TR-FDA-MIMO radar, according to the principle of time reversal, the original received signals are time reversed, phase conjugated, and retransmitted by the receiving array to illuminate the targets again. The back-propagated signals will focus on the targets, be reflected, and recorded by the transmitting array. The retransmitted signal is represented as

$$\begin{aligned} \mathbf{Y}_{TR}(t) &= \mathbf{Y}^*(-t) \\ &= \sum_{p=1}^P \mathbf{b}^*(\theta_p) \beta_p^* \mathbf{a}^H(r_p, \theta_p) \mathbf{X}^*(-t) + \mathbf{n}_y^*(-t) \end{aligned} \tag{18}$$

thus the final received signal is

$$\begin{aligned} \mathbf{Z}(t) &= \sum_{p=1}^P \mathbf{a}_0(\theta_p) \beta_p \mathbf{b}^T(\theta_p) \mathbf{Y}_{TR}(t) + \mathbf{n}_z(t) \\ &= \sum_{p=1}^P |\beta_p|^2 \mathbf{a}_0(\theta_p) \mathbf{b}^T(\theta_p) \mathbf{b}^*(\theta_p) \mathbf{a}^H(r_p, \theta_p) \mathbf{X}^*(-t) + \mathbf{n}(t), \end{aligned} \tag{19}$$

where $\mathbf{a}_0(\theta)$ is the TR receiving array manifold. $\mathbf{n}_z(t)$ is also a

WGN vector whose mean and variance are zero and σ^2 respectively, and $\mathbf{n}(t)$ is the accumulated noise which is given by

$$\mathbf{n}(t) = \sum_{p=1}^P \mathbf{a}_0(\theta_p) \beta_p \mathbf{b}^T(\theta_p) \mathbf{n}_y^*(-t) + \mathbf{n}_z(t). \quad (20)$$

Note that $\mathbf{a}_0(\theta)$ here actually acts as the receiving steering vector for TR signals, thus it is angle-dependent only and written as

$$\mathbf{a}_0(\theta) = [1, e^{j\varphi_{a_0}}, \dots, e^{j(M-1)\varphi_{a_0}}]^T, \quad (21)$$

where $\varphi_{a_0} = 2\pi d_T \sin \theta / \lambda_0$. Similar to (17), the matched filter output of the TR received signals is calculated as

$$\begin{aligned} \mathbf{Z}_{MF} &= E\{\mathbf{Z}(t)\mathbf{X}^T(-t)\} = N \sum_{p=1}^P |\beta_p|^2 \mathbf{a}_0(\theta_p) \mathbf{a}^H(r_p, \theta_p) + \mathbf{N} \\ &= \mathbf{N} \mathbf{A}_0 \mathbf{\Lambda} \mathbf{A}^H + \mathbf{N}, \end{aligned} \quad (22)$$

where \mathbf{N} is the matched filtering result of $\mathbf{n}(t)$, and \mathbf{A}_0 , $\mathbf{\Lambda}$, and \mathbf{A} are given by

$$\mathbf{A}_0 = [\mathbf{a}_0(\theta_1), \mathbf{a}_0(\theta_2), \dots, \mathbf{a}_0(\theta_p)], \quad (23a)$$

$$\mathbf{\Lambda} = \text{diag}(|\beta_1|^2, |\beta_2|^2, \dots, |\beta_p|^2), \quad (23b)$$

$$\mathbf{A} = [\mathbf{a}(r_1, \theta_1), \mathbf{a}(r_2, \theta_2), \dots, \mathbf{a}(r_p, \theta_p)], \quad (23c)$$

respectively.

To acquire the targets imaging spectra in the range-angle domain based on \mathbf{Z}_{MF} , we utilize the MUSIC algorithm that is commonly used in MIMO radar DOA estimation for favorable resolution performance. First, vectorization is performed to \mathbf{Z}_{MF} to obtain the virtual data vector as follows

$$\mathbf{z} = \text{vec}(\mathbf{Z}_{MF}) = N \sum_{p=1}^P |\beta_p|^2 \mathbf{a}_{TR}(r_p, \theta_p) + \mathbf{n}, \quad (24)$$

where $\text{vec}(\cdot)$ denotes the vectorization and $\mathbf{n} = \text{vec}(\mathbf{N})$. $\mathbf{a}_{TR}(r, \theta)$ is the TR joint transmitting-receiving steering vector defined as

$$\mathbf{a}_{TR}(r, \theta) = \mathbf{a}^*(r, \theta) \otimes \mathbf{a}_0(\theta), \quad (25)$$

with \otimes denoting the Kronecker product. Next, the covariance matrix of \mathbf{z} is solved and the eigenvalue decomposition (EVD) is conducted

$$\mathbf{R}_z = E\{\mathbf{z}\mathbf{z}^H\} = (\mathbf{U}_s | \mathbf{U}_n) \mathbf{\Sigma} (\mathbf{U}_s | \mathbf{U}_n)^H, \quad (26)$$

where \mathbf{U}_s , \mathbf{U}_n , and $\mathbf{\Sigma}$ are signal subspace, noise subspace, and diagonal matrix of eigenvalues, respectively. At last, target range and angle estimation are realized by searching the spectral peak for each point in the discretized range-angle domain

$$I(r, \theta) = [\mathbf{a}_{TR}^H(r, \theta) \mathbf{U}_n \mathbf{U}_n^H \mathbf{a}_{TR}(r, \theta)]^{-1}. \quad (27)$$

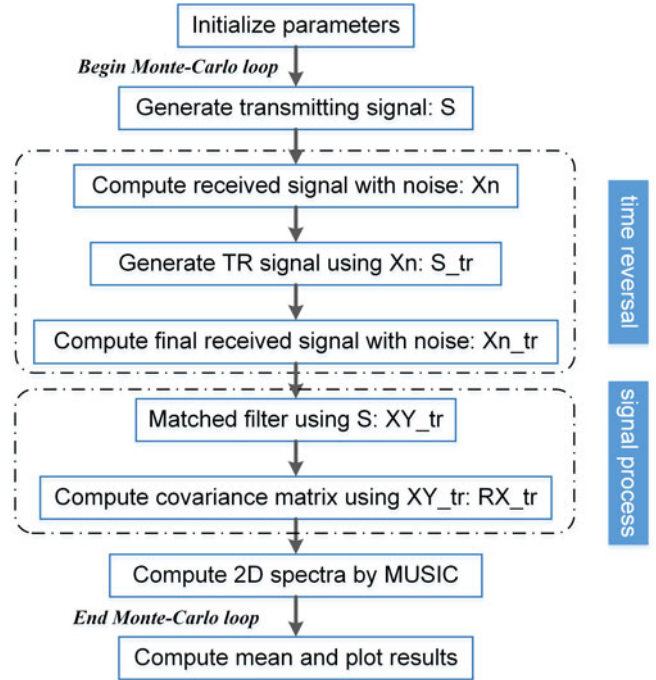


Fig. 3. Flow diagram of MATLAB simulation.

Numerical results and analysis

Simulation setup

In this section, we examine the performance of the proposed TR-FDA-MIMO radar by numerical simulations. Both single-target and multi-target cases are taken into account, and conventional FDA-MIMO results are provided for comparisons.

Simulation parameters are set as follows: the number of transmitting and receiving elements of the co-located radar are $M = 8$ and $N = 6$, respectively, the reference carrier frequency is $f_0 = 10$ GHz, the frequency increment is $\Delta f = 30$ KHz, the element spacing is set as $d_T = d_R = (1/2)\lambda_0$ to avoid grating lobes in angle dimension, and the number of sampling snapshots is $L = 50$. The scope of range and angle domains is $r \in [0, 5$ km] and $\theta \in [-90^\circ, 90^\circ]$, respectively. The Hadamard matrix is used to generate orthogonal modulation signal for radar waveform transmission. Numerical simulations are conducted via MATLAB R2013b and results are exported through 200 Monte-Carlo simulations. Figure 3 shows the flow diagram of the simulation.

Simulation results

At first, we investigate the range-angle estimation for a single target located at (2 km, 30°) with the signal-to-noise ratio (SNR) being -10 dB. The range-angle imaging spectra given by FDA-MIMO and TR-FDA-MIMO radars are shown in Figs 4(a) and 4(b), respectively, where spectra intensities are normalized and depicted in the form of dB. It can be seen that both FDA-MIMO and TR-FDA-MIMO radars realize joint range and angle estimation, namely, unambiguous target localization. However, it is obvious that TR-FDA-MIMO radar has a more focused imaging spot. To make a more detailed comparison, the normalized imaging resolution in range and angle dimensions of the two methods are plotted, as shown in Fig. 5. It can be observed

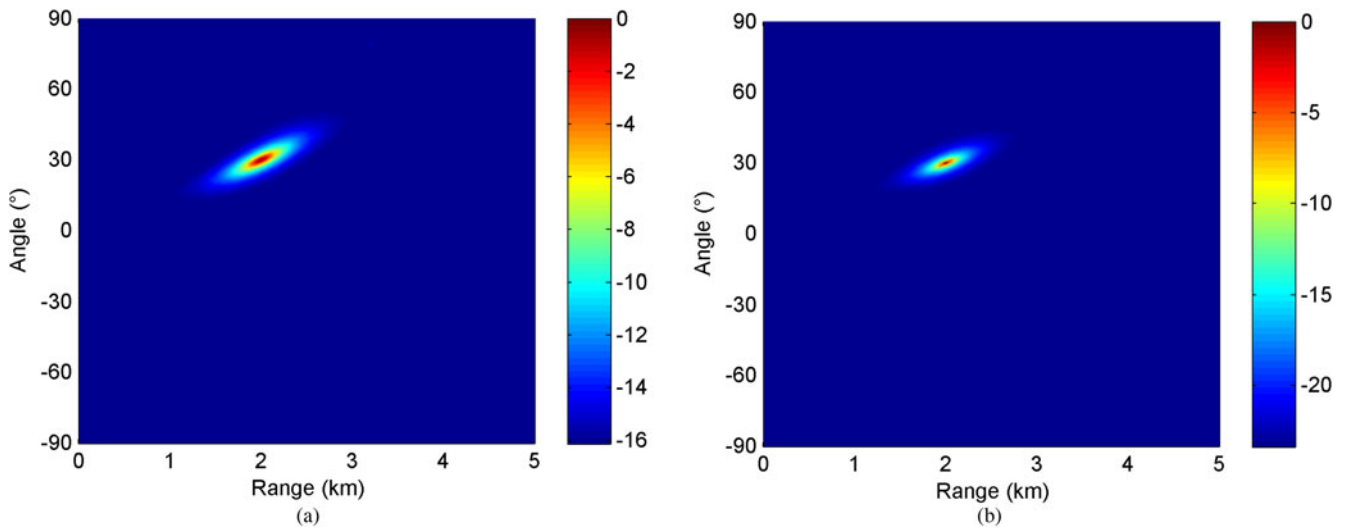


Fig. 4. Range-angle imaging spectra: (a) FDA-MIMO and (b) TR-FDA-MIMO.

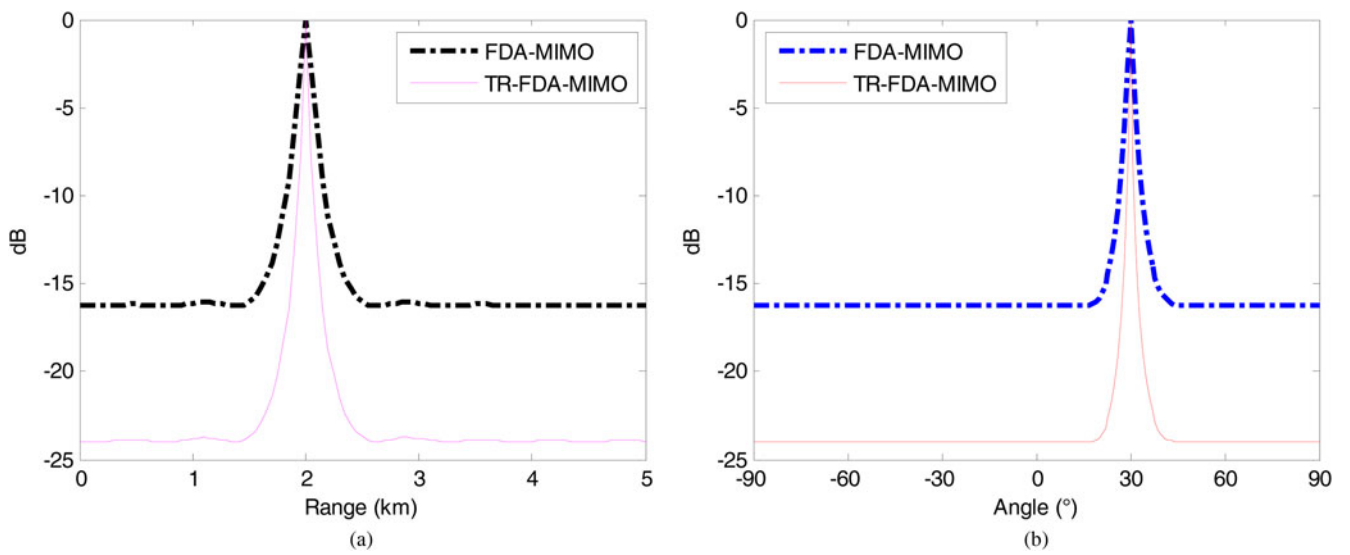


Fig. 5. Resolution comparison between FDA-MIMO and TR-FDA-MIMO: (a) range resolution and (b) angle resolution.

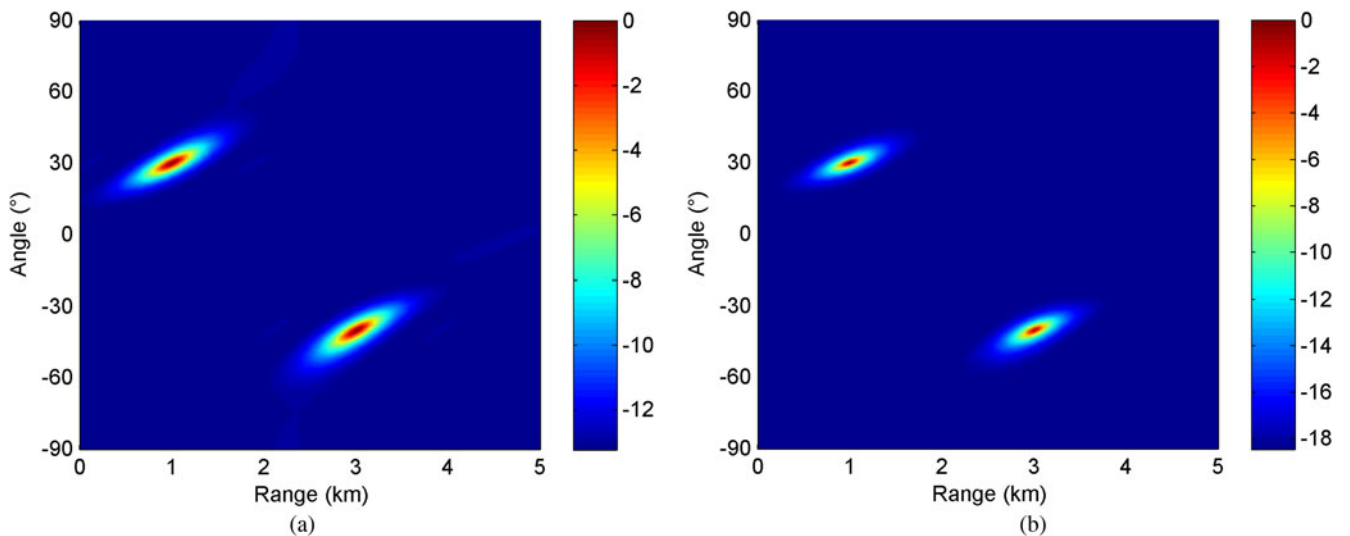


Fig. 6. Range-angle imaging spectra of two targets: (a) FDA-MIMO and (b) TR-FDA-MIMO.

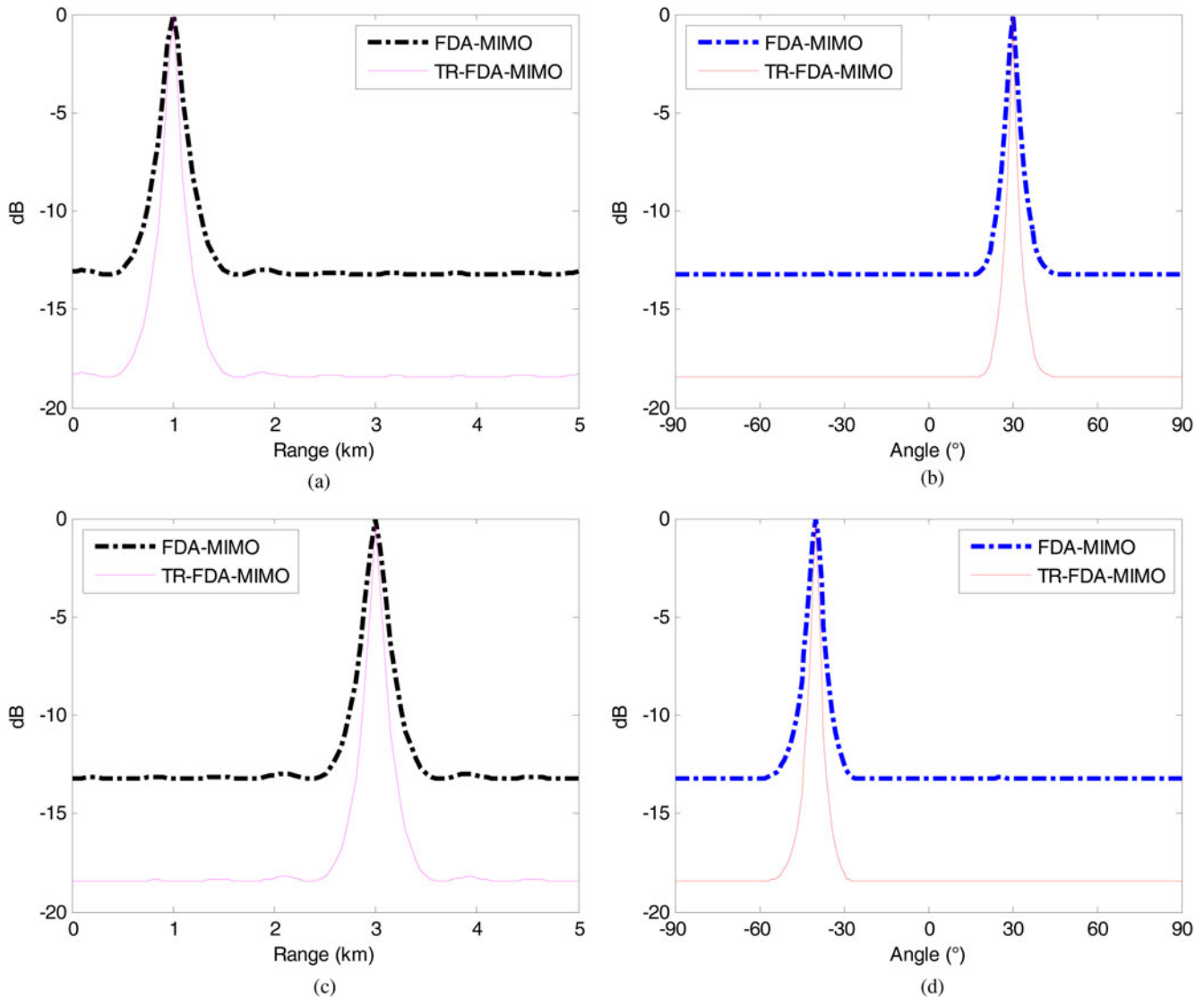


Fig. 7. Resolution comparison between FDA-MIMO and TR-FDA-MIMO: (a) range resolution for the target located at (1 km, 30°), (b) angle resolution for the target located at (1 km, 30°), (c) range resolution for the target located at (3 km, -40°), and (d) angle resolution for the target located at (3 km, -40°).

that by combining time reversal with FDA-MIMO radar, range and angle resolutions are both effectively enhanced, which means that more precise target detection can be achieved by the new approach.

Next, we study the multi-target case where two targets are located at (1 km, 30°) and (3 km, -40°), respectively, with SNR = -10 dB as well. The imaging results given by FDA-MIMO and TR-FDA-MIMO radars are demonstrated in Figs 6 (a) and 6(b), respectively. As we can see, these two methods realize range-angle imaging for the two targets, indicating the multi-target detecting capacity of FDA-MIMO radar. But still, the new TR-FDA-MIMO radar provides a preferable imaging result. The imaging resolution in range and angle dimensions of the two methods are compared in Fig. 7, where the superiority of the proposed method is further revealed.

Then, we consider the detection for three targets located at (2.5 km, -40°), (2.5 km, 15°), and (3 km, 30°), respectively, where two of them are located closely to each other. Figures 8 (a) and 8(b) show the imaging spectra obtained with SNR = 10 dB which represents the low-noise case, while Figs 8(c) and 8(d) show the imaging spectra obtained with SNR = -15 dB

which represents the high-noise case. It is observed that in the low-noise case, these two methods show excellent imaging results with TR-FDA-MIMO slightly outperforming FDA-MIMO. In the high-noise case, on the one hand, due to strong noise effects, the imaging performance of FDA-MIMO degenerates a lot, leading to a failure of resolving the two closely located targets. On the other hand, TR-FDA-MIMO still achieves accurate range-angle estimation for all the three targets in the strong noise condition. Moreover, the spatial half-power (-3 dB) profile of imaging spectra given by FDA-MIMO and TR-FDA-MIMO in the high-noise case is compared in Fig. 9, which clearly indicates the improvement of imaging performance brought by the proposed method.

At last, for robustness assessment, the root mean square error (RMSE) versus SNR curves of the two methods in range and angle estimation are plotted in Figs 10(a) and 10(b), respectively. It shows that the range and angle RMSEs of FDA-MIMO and TR-FDA-MIMO both reduce with the increase of SNR. As for range dimension, TR-FDA-MIMO has lower RMSE value when SNR is below 0 dB, and it has nearly the same estimation error with FDA-MIMO when SNR is above 0 dB. As for angle

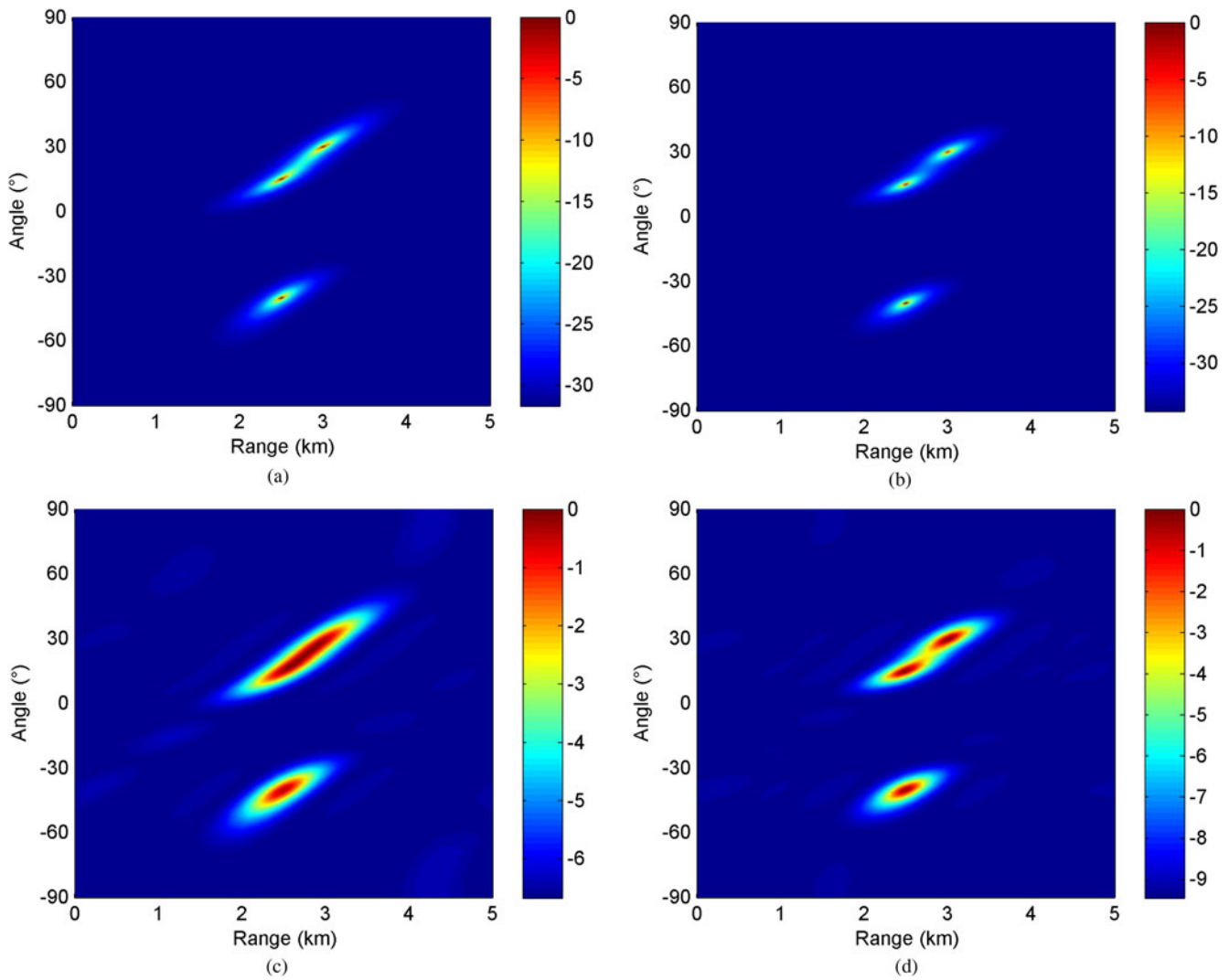


Fig. 8. Range-angle imaging spectra for three targets: (a) FDA-MIMO with SNR = 10 dB, (b) TR-FDA-MIMO with SNR = 10 dB, (c) FDA-MIMO with SNR = -15 dB, and (d) TR-FDA-MIMO with SNR = -15 dB.

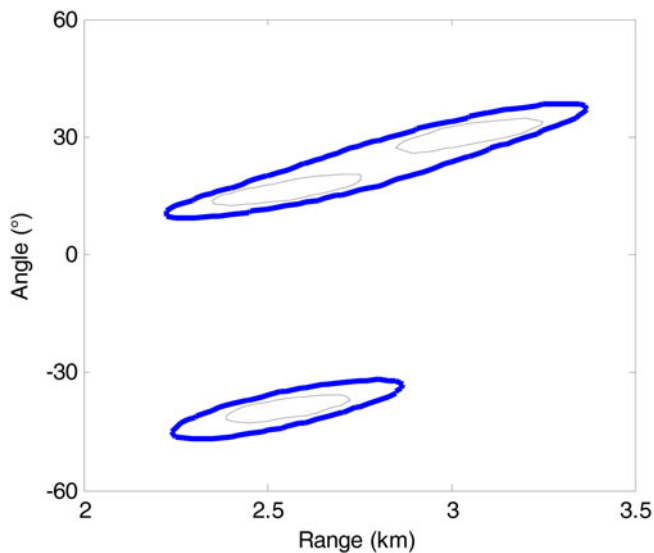


Fig. 9. The -3 dB profile of imaging spectra in the high-noise case. The blue thick profile corresponds to FDA-MIMO and the black thin profile corresponds to TR-FDA-MIMO.

dimension, TR-FDA-MIMO has lower RMSE value at each SNR, and the stronger the noise, the more the TR-FDA-MIMO has the superiority. The comparison results indicate that the robustness to the noise also can be effectively improved by utilizing the proposed TR-FDA-MIMO radar.

Conclusion

FDA-MIMO radar has received much attention in recent years for its range-dependent beampattern and increased DoFs. In this paper, we present a new FDA-MIMO radar that combines with time reversal to enhance radar performance in the joint range-angle estimation for far-field targets. The TR-FDA-MIMO signal model is established and the TR signal processing is analyzed. The resulting range-angle imaging spectra are solved by using the MUSIC algorithm. Numerical simulations are carried out to validate the effectiveness of the proposed method. Simulation results are compared with traditional FDA-MIMO radar and it turned out that the new TR-FDA-MIMO radar performs better in imaging resolution and robustness to the noise.

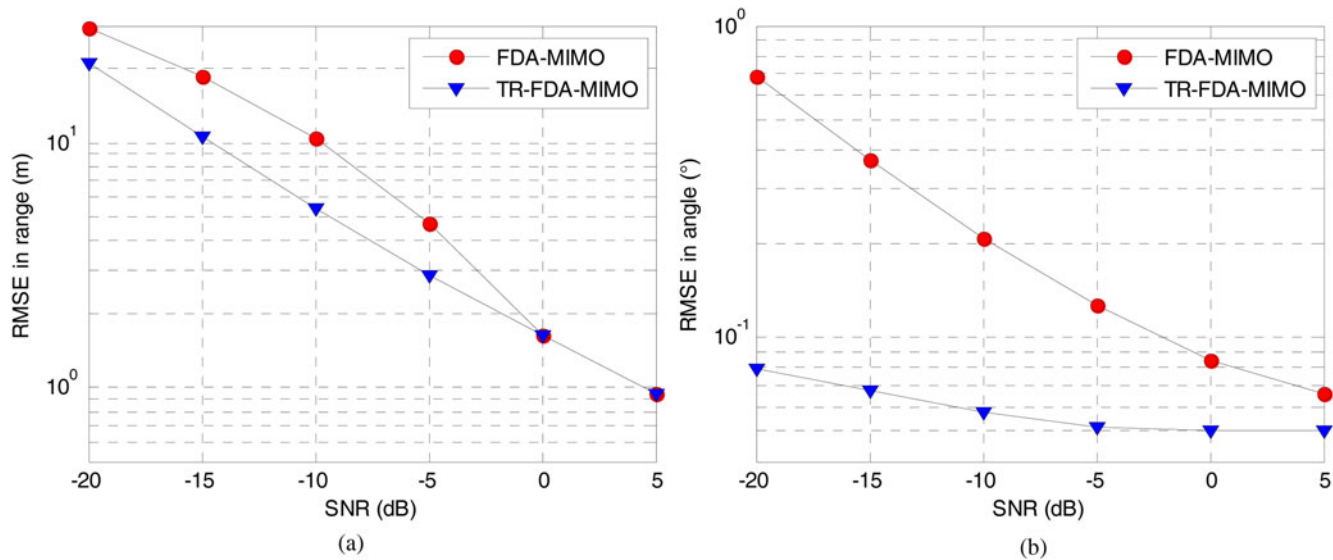


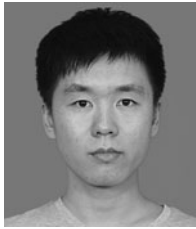
Fig. 10. RMSE comparison between FDA-MIMO and TR-FDA-MIMO: (a) in range dimension and (b) in angle dimension.

Furthermore, the used MUSIC algorithm requires the number of targets for imaging and its inherent spectrum searching causes huge computation. Therefore, more efficient imaging algorithm should be investigated in the future for reducing the computational complexity. Applying the TR-FDA-MIMO radar to moving targets tracking and conducting experimental verification also should be considered in future work.

Acknowledgement. This work was supported by the National Natural Science Foundation of China under Grant 61271331 and Grant 61571229.

References

- Li J and Stoica P (2007) MIMO radar with colocated antennas. *IEEE Signal Processing Magazine* **24**, 106–114.
- Akcakaya M and Nehorai A (2011) MIMO radar sensitivity analysis for target detection. *IEEE Transactions on Signal Processing* **7**, 3241–3250.
- Davis M, Showman G and Lanterman A (2014) Coherent MIMO radar: the phased array and orthogonal waveforms. *IEEE Aerospace and Electronic Systems Magazine* **29**, 76–91.
- Antonik P, Wicks MC, Griffiths HD and Baker CJ (2006) Frequency diverse array radars. *2006 IEEE Radar Conference*, Verona.
- Sammartino PF, Baker CJ and Griffiths HD (2013) Frequency diverse MIMO techniques for radar. *IEEE Transactions on Aerospace and Electronic Systems* **49**, 201–222.
- Wang WQ and Shao H (2014) Range-angle localization of targets by a double-pulse frequency diverse array radar. *Journal of Selected Topics in Signal Processing* **8**, 106–114.
- Secmen M, Demir S, Hizal A and Eker T (2007) Frequency diverse array antenna with periodic time modulated pattern in range and angle. *2007 IEEE Radar Conference*, Boston.
- Khan W, Qureshi IM and Saeed S (2015) Frequency diverse array radar with logarithmically increasing frequency offset. *IEEE Antennas and Wireless Propagation Letters* **14**, 499–502.
- Khan W and Qureshi IM (2014) Frequency diverse array radar with time-dependent frequency offset. *IEEE Antennas and Wireless Propagation Letters* **13**, 758–761.
- Yao AM, Wu W and Fang DG (2016) Frequency diverse array antenna using time-modulated optimized frequency offset to obtain time-invariant spatial fine focusing beampattern. *IEEE Transactions on Antennas and Propagation* **64**, 4434–4446.
- Yao AM, Rocca P, Wu W, Massa A and Fang DG (2017) Synthesis of time-modulated frequency diverse arrays for short-range multi-focusing. *IEEE Journal of Selected Topics in Signal Processing* **11**, 282–294.
- Wang Y, Li W, Huang G and Li JL (2017) Time-invariant range-angle-dependent beampattern synthesis for FDA radar targets tracking. *IEEE Antennas and Wireless Propagation Letters* **16**, 2375–2379.
- Chen B, Chen X, Huang Y and Guan J (2018) Transmit beampattern synthesis for the FDA radar. *IEEE Antennas and Wireless Propagation Letters* **17**, 98–101.
- Xu J, Liao G, Zhu S, Huang L and So HC (2015) Joint range and angle estimation using MIMO radar with frequency diverse array. *IEEE Transactions on Signal Processing* **63**, 3396–3410.
- Gao K, Wang WQ and Cai J (2016) Frequency diverse array and MIMO hybrid radar transmitter design via Cramér–Rao lower bound minimisation. *IET Radar, Sonar & Navigation* **10**, 1660–1670.
- Xiong J, Wang WQ and Gao K (2018) FDA-MIMO radar range-angle estimation: CRLB, MSE, and resolution analysis. *IEEE Transactions on Aerospace and Electronic Systems* **54**, 284–294.
- Lerosey G, De Rosny J, Tourin A, Derode A, Montaldo G and Fink M (2004) Time reversal of electromagnetic waves. *Physical Review Letters* **92**, 193904.
- Yavuz ME and Teixeira FL (2008) Space–frequency ultrawideband time-reversal imaging. *IEEE Transactions on Geoscience and Remote Sensing* **46**, 1115–1124.
- Ciuonzo D (2017) On time-reversal imaging by statistical testing. *IEEE Signal Processing Letters* **24**, 1024–1028.
- Odedo VC, Yavuz ME, Costen F, Himeno R and Yokota H (2017) Time reversal technique based on spatiotemporal windows for through the wall imaging. *IEEE Transactions on Antennas and Propagation* **65**, 3065–3072.
- Jin Y, Moura JMF and O'Donoghue N (2010) Time reversal in multiple-input multiple-output radar. *IEEE Journal of Selected Topics in Signal Processing* **4**, 210–225.
- Foroozan F, Asif A, Jin Y and Moura JMF (2011) Direction finding algorithms for time reversal MIMO radars. *2011 IEEE Statistical Signal Processing Workshop*, Nice.
- Liu M, Hu G, Fan B, Gu J and Li Z (2018) Time reversal MIMO radar for multi-targets DOA estimation. *2nd International Conference on Data Mining, Communications and Information Technology*, Shanghai.
- Sajjadih MHS and Asif A (2015) Compressive sensing time reversal MIMO radar: joint direction and Doppler frequency estimation. *IEEE Signal Processing Letters* **22**, 1283–1287.
- Zhang X, Xu L, Xu L and Xu DH (2010) Direction of departure (DOD) and direction of arrival (DOA) estimation in MIMO radar with reduced-dimension MUSIC. *IEEE Communications Letters* **14**, 1161–1163.



Tong Mu received the B.E. degree in electronic information engineering from the Nanjing University of Science and Technology in 2014. He is now pursuing the Ph.D. degree in information and communication engineering. His main research interests are antenna array, radar signal processing, and microwave imaging.



Yaoliang Song received the B.E., the M.E., and the Ph.D. degrees in electrical engineering from the Nanjing University of Science and Technology, in 1983, 1986, and 2000, respectively. He has been a researcher fellow at the Department of Engineering Science at the University of Oxford from September 2004 to September 2005. He now is a professor at the Nanjing University of Science and Technology.

His major research interests include UWB communications, UWB radar imaging, and advanced signal processing.